Robust Predictive Speed Control of SPMSM Drives With Algebraically Designed Weighting Factors

Xicai Liu, *Member, IEEE*, Jin Wang, *Member, IEEE*, Xiaonan Gao, *Member, IEEE*, Wei Tian, *Member, IEEE*, Libing Zhou, *Member, IEEE*, and Ralph Kennel, *Senior Member, IEEE*

***Abstract*—Predictive speed control (PSC) is a promising control strategy for high dynamic performance electrical drives. However, its implementation faces two challenges: the selection of weighting factors and the elimination of steady-state errors (SSEs). The weighting factors are commonly selected through trial-and-error, which is time consuming. Additionally, SSEs are frequently observed due to model uncertainties and parameter mismatches. Focusing on the aforementioned issues, this article proposes a PSC strategy for surface-mounted permanent-magnet synchronous motor drives, where the weighting factors are designed algebraically and SSEs are eliminated. The weighting factor design process is illustrated through rearranging the equivalent speed tracking error. The SSEs are eliminated by incorporating integral terms into the cost function. The performance of the proposed strategy is validated through comparative experiments with field-oriented control and adaptive integral sliding-mode predictive control. The results demonstrate the effectiveness of the designed weighting factors and the robustness of the system.**

***Index Terms*—Predictive speed control (PSC), robustness improvement, surface -mounted permanent-magnet synchronous motor (SPMSM), weighting factor design.**

I. Introduction

RECENTLY, model predictive control (MPC) has been widely investigated in electrical drives, owing to its ability to handle constraints while maintaining a high dynamic performance [1], [2]. Compared to field-oriented control (FOC) and direct torque control, MPC can achieve faster or at least the same dynamic performance. Meanwhile, the safe operation of the motor is ensured and overcurrent is avoided [3], [4].

The most widely known MPC control schemes in electrical drives are predictive current control (PCC) and predictive torque control (PTC), while predictive speed control (PSC) appears as an emerging control strategy. PCC and PTC are used in the inner control loop cascaded with a proportional-integral (PI) speed controller, while this PI speed controller is replaced with the predictive controller in PSC. PSC improves the speed dynamic performance tremendously, thanks to its high bandwidth and the possibility of eliminating the cascaded structure [5].

For PSC without cascaded structure, a single cost function is used, where weighting factors assign the respective importance to the speed and current tracking errors. However, these tracking errors possess highly different magnitudes, which challenges the selection of weighting factors. The selection process is often tedious since design guidelines are unavailable.

Unfortunately, the weighting factor design in PSC attracts insufficient attention. In fact, major contributions on the weighting factor design are confined to PTC. Even worse, the weighting factor design in PSC is far more challenging than that in PTC. The solutions proposed in PTC *cannot* be directly applied to PSC, which include normalization of the variables [6], [7], algebraic tuning [8], [9], control of the respective vector [10], [11], weighted ranking of separate cost functions [12], [13], sequential cost function evaluation [14], [15], and artificial intelligence [16], [17]. The magnitude differences between the rotor speed and currents are extremely large, which means the tuning process based on normalization of variables is far more time consuming in PSC. The models used for optimization between PTC and PSC are also different, which poses questions on whether algebraic tuning or the control of the respective vector is possible. Weighted ranking of cost functions and sequential cost function evaluation may fail due to the large time constant difference between the speed and current. The tuning of weighting factors through artificial intelligence requires an optimization criterion. Obviously, the optimization criterion for PTC differs from that for PSC.

The weighting factors in PSC are mostly designed through the trial-and-error process [18], [19], [20], [21], while the elimination of them is also possible [22]. In [18], [19], [20], and [21], the weighting factors are selected from a large variation range, which means the tuning process is nontrivial. To eliminate the weighting factors, reference voltages are calculated based on the dead-beat (DB) concept and the voltage tracking errors are evaluated in [22]. However, DB ignores the penalty on inverter switch transitions and its performance hinges on the sampling frequency.

Manuscript received 12 April 2022; revised 25 June 2022; accepted 5 August 2022. Date of publication 16 August 2022; date of current version 6 September 2022. Recommended for publication by Associate Editor Jin Ye. *(Corresponding author: Jin Wang.)*

Xicai Liu, Xiaonan Gao, Wei Tian, and Ralph Kennel are with the Chair of High-Power Converter Systems, Technical University of Munich (TUM), 80333 Munich, Germany (e-mail: xicai.liu@tum.de; xiaonan.gao@tum.de; wei.tian@tum.de; ralph.kennel@tum.de).

Jin Wang and Libing Zhou are with the State Key Laboratory of Advanced Electromagnetic Engineering and Technology and School of Electrical and Electronic Engineering, Huazhong University of Science and Technology, Wuhan 430074, China (e-mail: hustwj@126.com; zlb@mail.hust.edu.cn).

Color versions of one or more figures in this article are available at https://doi.org/10.1109/TPEL.2022.3198748.

Digital Object Identifier 10.1109/TPEL.2022.3198748

Apart from weighting factor design issue, PSC also suffers from model uncertainties and parameter mismatches. Steady-state errors (SSEs) are commonly observed. To eliminate SSEs, and thus, improve the robustness of PSC, researchers have proposed various solutions such as disturbance estimation [23], estimation of unknown parameters [24], adaptive integral sliding-mode surface [25], and augmented model [26]. The lumped disturbances are estimated with a sliding mode observer in [23], while the unknown parameters are estimated with adaptive laws in [24]. The estimation of disturbance and parameters improves the robustness, but also leads to a complex control structure. On the other hand, integral actions can be used alternatively with simple control structure. Adaptive integral sliding-mode predictive control (AISMPC) with cascaded structure has been proposed in [25] to improve the robustness of the system. In the speed loop, the integral of the speed error is used in designing the sliding-mode surface, which requires antiwindup mechanism and careful design of the integral coefficients. Otherwise, speed overshoots will occur. In [26], integral actions are incorporated by using an augmented model to eliminate the SSEs, which is achieved through the incremental part of the model.

In this article, a PSC strategy is proposed to facilitate the selection of the weighting factors and eliminate the SSEs. The contributions of this article are as follows.

1) The weighting factors for the tracking errors are designed algebraically, which can be directly used, even in the presence of some parameter mismatches.
   Quite the opposite, the conventional tuning procedure fails to provide any insight of how to weigh the control performance of different variables. Without such insight, the tuning procedure is time consuming, where trial-and-error is the only option.
2) Integral terms are incorporated into the cost function without incurring speed overshoots while eliminating the SSEs, where the integral action is only activated in a predefined operation range.
   In contrast, existing solutions with integral actions are achieved through the augmented model or the integral of the speed error. For the augmented model, no configuration option is available for the integral action. For the latter case, large speed overshoots could occur and elaborate antiwindup mechanism is required.

This article is organized as follows. First, the surface-mounted permanent-magnet synchronous motor (SPMSM) model is given and the principle of PSC based on the equivalent speed tracking error is illustrated. Second, the proposed robust PSC strategy with algebraic weighting factor design is described in detail. Third, comparative experiments are implemented to validate the proposed PSC strategy. Finally, conclusion is drawn based on the experimental results and theoretical analysis.

II. SPMSM Model and the Principle of PSC Based on the Equivalent Speed Tracking Error

In this section, an SPMSM model in continuous and discrete form is first introduced. Thereafter, the principle of PSC based on the equivalent speed tracking error is briefly described.

A. SPMSM Model

The system dynamics of the SPMSM in the synchronous rotating d-q frame can be expressed as

$$\begin{cases} \frac{d}{dt}i_q = -\frac{R_s}{L_s}i_q + \frac{u_q}{L_s} - \omega_e i_d - \frac{\omega_e \psi_f}{L_s} \\ \frac{d}{dt}i_d = -\frac{R_s}{L_s}i_d + \frac{u_d}{L_s} + \omega_e i_q \\ J_m \frac{d\omega_m}{dt} = T_e - T_L \end{cases} \tag{1}$$

where i_d and i_q are the d-axis and q-axis stator current, respectively. u_d and u_q symbolize the stator voltage on the d-axis and q-axis, respectively. R_s represents the stator resistance, L_s is the stator inductance, ψ_f is the rotor flux linkage, and J_m is the moment of rotor inertia. ω_e and ω_m stand for the electrical and the mechanical angular rotor speed, respectively. T_e is the electromagnetic torque and $T_e = \frac{3}{2}n_p\psi_f i_q$, n_p is the pole pair number, and T_L is the load torque.

In practical applications, (1) can be discretized with the forward Euler method assuming a relatively small sampling time T_s. For notational simplicity, the discrete current equations are expressed in matrix and vector forms as

$$\boldsymbol{i}_{dq}(k+1) = \boldsymbol{A}_m(k)\boldsymbol{i}_{dq}(k) + \boldsymbol{B}_m\boldsymbol{U}_{dq}(k) + \boldsymbol{D}_m(k) \tag{2}$$

where

$$\boldsymbol{i}_{dq}(k+1) = \begin{bmatrix} i_q(k+1) \\ i_d(k+1) \end{bmatrix}, \boldsymbol{U}_{dq}(k) = \begin{bmatrix} u_q(k) \\ u_d(k) \end{bmatrix}$$
$$\boldsymbol{A}_m(k) = \begin{bmatrix} 1 - \frac{R_s T_s}{L_s} & -\omega_e(k)T_s \\ \omega_e(k)T_s & 1 - \frac{R_s T_s}{L_s} \end{bmatrix}, \boldsymbol{B}_m = \begin{bmatrix} \frac{T_s}{L_s} & 0 \\ 0 & \frac{T_s}{L_s} \end{bmatrix}$$
$$\boldsymbol{D}_m(k) = \begin{bmatrix} -\frac{\psi_f}{L_s}\omega_e(k)T_s \\ 0 \end{bmatrix}.$$

The discrete mechanical equation is expressed as

$$\omega_m(k+1) = \omega_m(k) + \frac{T_s}{J_m}\left(\frac{T_e(k+1) + T_e(k)}{2} - T_L(k)\right). \tag{3}$$

B. Principle of PSC Based on the Equivalent Speed Tracking Error

In this section, the PSC strategy based on the equivalent speed tracking error is introduced. The equivalent speed tracking error is defined as [24], [27]

$$e_\omega = \eta_m\omega_{\text{err}} + \dot{\omega}_{\text{err}} \tag{4}$$

where ω_{err} is the electrical angular speed tracking error and $\omega_{\text{err}} = \omega_e^* - \omega_e$. ω_e^* is the electrical angular reference speed, η_m is a scaling coefficient, and $\eta_m > 0$.

At time instant k, e_ω can be expressed as

$$e_\omega(k) = \eta_m(\omega_e^*(k) - \omega_e(k)) - \frac{n_p}{J_m}(T_e(k) - T_L(k)). \tag{5}$$

In PSC based on equivalent speed tracking error, e_ω and i_d are controlled simultaneously. Taking one-step delay into account, the cost function can be designed as

$$J = (\boldsymbol{x}^* - \boldsymbol{x}^p(k+2))^T\boldsymbol{W}(\boldsymbol{x}^* - \boldsymbol{x}^p(k+2)) + k_u\Delta\boldsymbol{U}_{dq}(k+1)^T\Delta\boldsymbol{U}_{dq}(k+1) \tag{6}$$

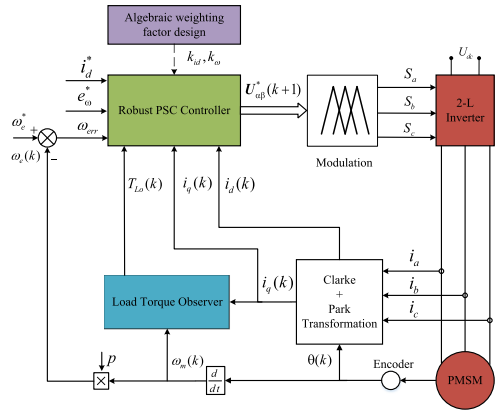

Fig. 1. Control diagram of the proposed robust PSC strategy with algebraic weighting factor design.

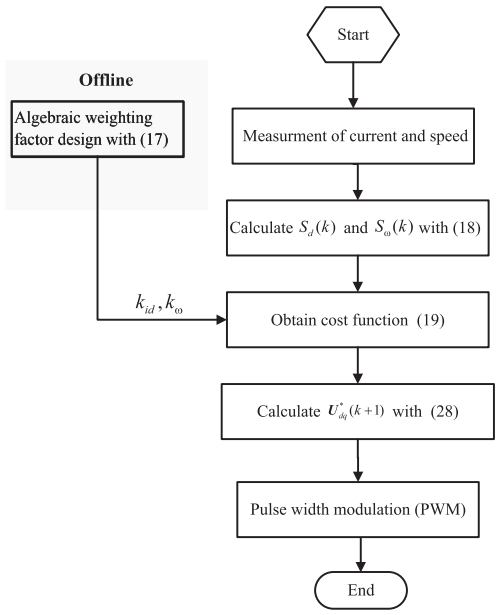

Fig. 2. Control flow of the proposed robust PSC strategy with algebraic weighting factor design.

subject to

$$(i_d^p(k+2))^2 + (i_q^p(k+2))^2 \le i_{\max}^2$$

$$(u_d(k+1))^2 + (u_q(k+1))^2 \le u_{\max}^2$$

where $\boldsymbol{x}^* = [e_\omega^*(k+2), i_d^*(k+2)]^T$, e_ω^* is the reference for e_ω, and i_d^* is the d-axis current reference. $\boldsymbol{x}^p(k+2)$ is the predicted vector of $\boldsymbol{x}$ at time instant $k+2$ and $\boldsymbol{x}^p(k+2) = \begin{bmatrix} e_\omega^p(k+2) \\ i_d^p(k+2) \end{bmatrix}$. $\boldsymbol{W}$ is the weighting factor matrix for the tracking errors and $\boldsymbol{W} = \begin{bmatrix} k_\omega^2 & 0 \\ 0 & k_{id}^2 \end{bmatrix}$, and k_u is used to penalize the variation of control actions. $\Delta \boldsymbol{U}_{dq}(k+1) = \boldsymbol{U}_{dq}(k+1) - \boldsymbol{U}_{dq}(k)$. $i_{\max}$ and $u_{\max}$ are the current and voltage magnitude limit, respectively.

III. Proposed PSC Strategy

In this section, we propose a robust PSC strategy with algebraically designed weighting factors. First, the algebraic weighting factors are derived through the rearrangement of e_ω. Second, integral terms are designed and incorporated into the cost function to eliminate the SSEs. Third, the calculation of the reference voltage is presented. Theoretical analysis of the integral terms is given in Appendix A2.

The block diagram and the control flow of the proposed PSC are shown in Figs. 1 and 2, respectively. The reference voltage vector $\boldsymbol{U}_{\alpha\beta}^*(k+1)$ is calculated by the controller, and then, synthesized through pulsewidth modulation. Note that load torque observer is used to estimate the load torque, which is required in calculating e_ω.

A. Algebraic Weighting Factor Design

Similar to (5), the equivalent speed tracking error e_ω at time instant $k+2$ can be predicted as

$$e_\omega^p(k+2) = \eta_m\left(\omega_e^*(k+2) - \omega_e^p(k+2)\right) - \frac{n_p}{J_m}(T_e^p(k+2) - T_L(k+2)). \quad (7)$$

The electrical rotor angular speed at time instant $k+2$ can be predicted as

$$\omega_e^p(k+2) = \omega_e^p(k+1) + \frac{n_p T_s}{J_m}\left(\frac{T_e^p(k+2)+T_e^p(k+1)}{2} - T_L(k+1)\right). \quad (8)$$

Assuming the load torque is varying slowly (i.e., $T_L(k+2) = T_L(k+1) = T_L$) and substitute (8) into (7), $e_\omega^p(k+2)$ is calculated as

$$e_\omega^p(k+2) = \eta_m(\omega_e^*(k+2) - \omega_e^p(k+1)) + \frac{n_p(\eta_m T_s + 1)}{J_m}T_L - \frac{n_p \eta_m T_s}{2J_m}T_e^p(k+1) - \frac{n_p(\eta_m T_s + 2)}{2J_m}T_e^p(k+2). \quad (9)$$

A minor modification of (9) yields

$$e_\omega^p(k+2) = \frac{(\eta_m T_s + 2)}{2J_m}(S_T - n_p T_e^p(k+2)) \quad (10)$$

where

$$S_T = \frac{2J_m\eta_m}{2+\eta_m T_s}(\omega_e^*(k+2) - \omega_e^p(k+1)) + \frac{2n_p(\eta_m T_s+1)}{(2+\eta_m T_s)}T_L - \frac{n_p\eta_m T_s}{(2+\eta_m T_s)}T_e^p(k+1).$$

As can be seen from (10), S_T is related to the scaled electrical speed tracking error (the first term in S_T), the load torque T_L as well as the predicted electromagnetic torque $T_e^p(k+1)$. Neither $T_e^p(k+1)$ nor T_L can be actively controlled. $T_e^p(k+1)$ was already determined in the last sampling interval and T_L is the

external disturbance. It implies that $e_\omega^p(k+2)$ can be controlled only through $T_e^p(k+2)$.

Note that the magnitude of S_T is extremely large during acceleration and deceleration. Large $T_e^p(k+2)$ is required to counteract S_T, which could lead to overcurrent. To avoid such scenario, a saturation function can be used to restrict the magnitude of S_T as

$$\text{sat}(S_T) = \begin{cases} S_T & \text{if } |S_T| < S_T^{\max} \\ S_T^{\max} & \text{else} \end{cases} \tag{11}$$

where $S_T^{\max}$ is the saturated value of S_T. $S_T^{\max}$ can be designed based on the motor parameters. For instance, $S_T^{\max}$ can be set to $1.5 n_p T_{eN}$, where T_{eN} is the rated torque.

Replace S_T with $\text{sat}(S_T)$ in (10), the magnitude of $e_\omega^p(k+2)$ can also be restricted

$$e_{\omega,sat}^p(k+2) = \frac{(2+\eta_m T_s)}{2J_m}(sat(S_T) - n_p T_e^p(k+2)). \tag{12}$$

For the SPMSM, the electromagnetic torque is only related to the q-axis current

$$T_e^p(k+2) = \frac{3}{2} n_p \psi_f i_q^p(k+2). \tag{13}$$

Substitute (13) into (12), we have

$$e_{\omega,\text{sat}}^p(k+2) = \frac{3n_p^2\psi_f(2+\eta_m T_s)}{4J_m} \times \left(\frac{2}{3n_p^2\psi_f} \text{sat}(S_T) - i_q^p(k+2) \right). \tag{14}$$

By dividing the coefficient $\left(\frac{3n_p^2\psi_f(2+\eta_m T_s)}{4J_m}\right)^2$ with respect to $e_{\omega,\text{sat}}^p(k+2)$, the cost function with algebraic weighting factors is obtained as follows:

$$J = \left(\frac{4J_m}{3n_p^2\psi_f(2+\eta_m T_s)} \right)^2 (e_{\omega,sat}^p(k+2))^2 + (e_d^p(k+2))^2 + k_u \Delta \boldsymbol{U}_{dq}(k+1)^T \Delta \boldsymbol{U}_{dq}(k+1). \tag{15}$$

Note that

$$e_d^p(k+2) = i_d^*(k+2) - i_d^p(k+2) \tag{16}$$

where $i_d^p(k+2)$ is the predicted value of i_d at time instant $k+2$.

So far, the algebraic design of the weighting factor is achieved. As seen in (15), the weighting factor matrix $\boldsymbol{W}$ is

$$\boldsymbol{W} = \begin{bmatrix} \left(\frac{4J_m}{3n_p^2\psi_f(2+\eta_m T_s)}\right)^2 & 0 \\ 0 & 1 \end{bmatrix}. \tag{17}$$

It should be clarified that the algebraic weighting factor design is different from the adoption of a per-unit system. The per-unit system could reduce the magnitude difference between e_ω and i_d. However, the per-unit system does not assign adequate importance to each control variable. Weighting factors are still required to obtain satisfactory steady-state performance, even if a per-unit system is used.

Remark 1: For MPC, including PSC, some knowledge of the model is necessary or even compulsory. The proposed PSC strategy merely uses such knowledge to calculate the weighting factors, because the parameters J_m and ψ_f are also used in the prediction and optimization. Thus, the requirement of known parameters is not the limitation of the proposed strategy.

B. Incorporation of Integral Terms Into the Cost Function to Eliminate the SSEs

In cost function (15), the weighting factors can be easily designed. However, SSEs in ω_m and i_d are commonly observed due to model uncertainties and parameter mismatches. To eliminate these SSEs, integral actions can be adopted.

For convenience, the integral of e_ω and e_d are defined as $S_\omega(k)$ and $S_d(k)$ as follows:

$$\begin{cases} S_\omega(k) = S_\omega(k-1) + (e_\omega(k) - e_\omega(k-1)) + \mu_\omega e_\omega(k) T_s \\ S_d(k) \ = S_d(k-1) + (e_d(k) - e_d(k-1)) + \mu_d e_d(k) T_s \end{cases} \tag{18}$$

where μ_ω and μ_d are the integral coefficients.

In this article, $S_\omega(k)$ and $S_d(k)$ are incorporated into the cost function:

$$J = \left(\frac{4J_m}{3n_p^2\psi_f(2+\eta_m T_s)} \right)^2 (e_{\omega,\text{sat}}^p(k+2) + S_\omega(k))^2 + (e_d^p(k+2) + S_d(k))^2 + k_u \Delta \boldsymbol{U}_{dq}(k+1)^T \Delta \boldsymbol{U}_{dq}(k+1). \tag{19}$$

To avoid overshoots and facilitate the design of the integral coefficients, the integral actions are activated only in a predefined range ε as

$$\mu_\omega = \begin{cases} 0, & |(\omega_e^* - \omega_e)/\omega_e^*| > \varepsilon \\ \mu_\omega^*, & \text{else} \end{cases}$$
$$\mu_d = \begin{cases} 0, & |(\omega_e^* - \omega_e)/\omega_e^*| > \varepsilon \\ \mu_d^*, & \text{else} \end{cases} \tag{20}$$

where μ_ω^* and μ_d^* are the set values of μ_ω and μ_d, respectively.

The design of ε is easy, because load torque observer is used and the feedback gain of PSC is high. By assuming $\dot{\omega}_{\text{err}} \approx 0$ at steady state, we have $e_\omega^p(k+2) \approx \eta_m \omega_{\text{err}}(k) + \Delta f_\omega$, where Δf_ω is the model error in the mechanical equation. Δf_ω can be neglected since load torque observer is used. Therefore, the control of $e_\omega^p(k+2)$ and $\omega_{\text{err}}(k)$ are almost equal at steady state. The feedback gain of PSC is high, which means $\omega_{\text{err}}(k)$ is controlled with a high-gain controller. The result is that $\omega_{\text{err}}(k)$ is not large even without integral action. It means that a small ε can be used. Based on multiple simulations and experiments, $\varepsilon = 0.05$ commonly suffices.

Remark 2: $S_\omega(k)$ is formed with the integral of e_ω, which has advantage over the integral of ω_{err}. Compared to ω_{err}, e_ω decays much faster, which means e_ω enters steady-state, while ω_{err} is still large. By setting ε small (e.g., 0.05) and incorporate the integral term $S_\omega(k)$ into the cost function, speed overshoots can be avoided while eliminating the speed SSEs. The activation of the integral action within a predefined operation range ε has been proposed in [28] for PCC, but in a more generalized form.

C. Calculation of the Reference Voltage

As can be seen from (14), the speed control in the SPMSM can be accomplished through the control of $i_q^p(k+2)$. Since $i_d^p(k+2)$ is also simultaneously controlled in (15), the current vector is controlled in the proposed PSC. To calculate the reference voltage, current equations are given in an incremental vector form as follows:

$$\Delta \boldsymbol{i}_{dq}(k+1) = \boldsymbol{A}_m(k)\Delta \boldsymbol{i}_{dq}(k) + \boldsymbol{B}_m \Delta \boldsymbol{U}_{dq}(k) + \Delta \boldsymbol{D}_m(k) \quad (21)$$

where

$$\begin{aligned} \Delta \boldsymbol{i}_{dq}(k+1) &= \boldsymbol{i}_{dq}(k+1) - \boldsymbol{i}_{dq}(k) \\ \Delta \boldsymbol{U}_{dq}(k) &= \boldsymbol{U}_{dq}(k) - \boldsymbol{U}_{dq}(k-1) \\ \Delta \boldsymbol{D}_m(k) &= \boldsymbol{D}_m(k) - \boldsymbol{D}_m(k-1). \end{aligned}$$

Based on (21), the current vector at time instant $k+2$ is predicted as

$$\boldsymbol{i}_{dq}^p(k+2) = \boldsymbol{i}_{dq}^p(k+1) + \boldsymbol{A}_m(k)\Delta \boldsymbol{i}_{dq}^p(k+1) + \boldsymbol{B}_m \Delta \boldsymbol{U}_{dq}(k+1) + \Delta \boldsymbol{D}_m(k+1). \quad (22)$$

Substitute (22) into (19), we obtain the cost function where $\Delta \boldsymbol{U}_{dq}(k+1)$ is the decision variable

$$\begin{aligned} J = {} & \Delta \boldsymbol{U}_{dq}^T(k+1)\boldsymbol{\Phi}\Delta \boldsymbol{U}_{dq}(k+1) \\ & - 2\Delta \boldsymbol{U}_{dq}^T(k+1)\boldsymbol{B}_m^T \boldsymbol{W}\boldsymbol{\Theta}(k+1) \\ & + (\boldsymbol{\Theta}^T(k+1))\boldsymbol{W}(\boldsymbol{\Theta}(k+1)) \end{aligned} \quad (23)$$

where

$$\boldsymbol{\Phi} = \boldsymbol{B}_m^T \boldsymbol{W} \boldsymbol{B}_m + k_u \boldsymbol{I}_2,$$

$$\boldsymbol{\Theta}(k+1) = \boldsymbol{S}_{dq}^* - \boldsymbol{i}_{dq}^p(k+1) - \boldsymbol{A}_m(k)\Delta \boldsymbol{i}_{dq}^p(k+1) - \Delta \boldsymbol{D}_m(k+1)$$

$$S_{dq}^* = \begin{bmatrix} \frac{4J_m}{3n_p^2\psi_f(2+\eta_m T_s)} S_\omega(k) + \frac{2}{3n_p^2\psi_f} sat(S_T) \\ S_d(k) \end{bmatrix}.$$

Since $\boldsymbol{\Phi}$ is positive definite, J can be minimized if $\Delta \boldsymbol{U}_{dq}$ satisfies the following condition:

$$\frac{\partial J}{\partial \Delta \boldsymbol{U}_{dq}} = 2\boldsymbol{\Phi}\Delta \boldsymbol{U}_{dq}(k+1) - 2\boldsymbol{B}_m^T \boldsymbol{W}\boldsymbol{\Theta}(k+1) = 0. \quad (24)$$

By solving (24), the unconstrained optimal incremental voltage can be expressed as

$$\Delta \boldsymbol{U}_{dq,\text{unc}}(k+1) = \boldsymbol{\Phi}^{-1}\boldsymbol{B}_m^T \boldsymbol{W}\boldsymbol{\Theta}(k+1). \quad (25)$$

The unconstrained reference voltage is

$$\boldsymbol{U}_{dq,\text{unc}}(k+1) = \Delta \boldsymbol{U}_{dq,\text{unc}}(k+1) + \boldsymbol{U}_{dq}(k). \quad (26)$$

In case of inactive voltage constraints, i.e., $\boldsymbol{U}_{dq,\text{unc}}(k+1)$ is within the inner circle of the voltage hexagon, the actual reference voltage is $\boldsymbol{U}_{dq,\text{unc}}(k+1)$. Otherwise, the unconstrained reference voltage should be modified

$$\boldsymbol{U}_{dq,\text{cons}}(k+1) = \begin{bmatrix} \frac{U_{dc}}{\sqrt{3}} \frac{|u_q(k)+\Delta u_{q,\text{unc}}(k+1)|}{\|\boldsymbol{U}_{dq}(k)+\Delta \boldsymbol{U}_{dq,unc}(k+1)\|} \\ \frac{U_{dc}}{\sqrt{3}} \frac{|u_d(k)+\Delta u_{d,unc}(k+1)|}{\|\boldsymbol{U}_{dq}(k)+\Delta \boldsymbol{U}_{dq,unc}(k+1)\|} \end{bmatrix} \quad (27)$$

where U_{dc} is the dc-link voltage.

The reference voltage $\boldsymbol{U}_{dq}^*(k+1)$ in the synchronous rotating frame can be expressed as

$$\boldsymbol{U}_{dq}^*(k+1) = \begin{cases} \boldsymbol{U}_{dq,\text{unc}}(k+1) & \text{if} \frac{\|U_{dq,unc}(k+1)\|}{U_{\text{dc}}/\sqrt{3}} < 1 \\ \boldsymbol{U}_{dq,\text{cons}}(k+1) & \text{else.} \end{cases} \quad (28)$$

By applying the inverse Park transformation to $\boldsymbol{U}_{dq}^*(k+1)$, we obtain the reference voltage $\boldsymbol{U}_{\alpha\beta}^*(k+1)$ in the stationary frame.

Remark 3: In (27), the magnitude of $\boldsymbol{U}_{dq,\text{unc}}(k+1)$ is simply restricted to $\frac{U_{\text{dc}}}{\sqrt{3}}$ while maintaining the phase angle unchanged. The reason is to keep the algorithm as simple as possible. If necessary, a quadratic program (QP) solver can be used to maintain the reference voltage within the voltage hexagon, which is out of the scope of this article.

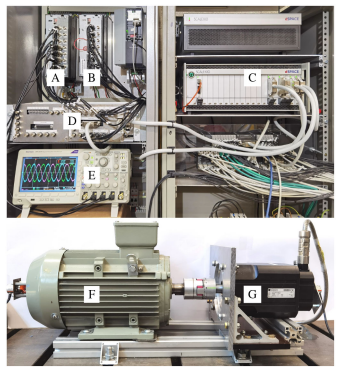

Fig. 3. Setup of the electrical drives testbench. A: SEW Inverter for SPMSM, B: SEW Inverter for load induction machine (IM), C: dSPACE SCALEXIO real-time control system, D: Interface, E: Oscilloscope, F: IM, and G: PMSM.

IV. Experimental Results

This section validates the performance of the proposed PSC experimentally, where both the steady-state and dynamic performance are examined. Comparative experiments with FOC and AISMPC [25] are also implemented. Fig. 3 shows the test bench, where an SPMSM and an induction motor serve as the test motor and load motor, respectively. Both motors are fed by SEW inverters controlled by a dSPACE SCALEXIO real-time control system. For the load motor, the torque and flux are controlled by PI controllers. Nominal parameters of the SPMSM are listed in Table I.

The sampling time is 100 μs and the dc-link voltage is 570 V. Carrier-based pulsewidth modulation (CB-PWM) with a carrier frequency of 10 kHz is used to synthesize the reference voltage. The current magnitude in the proposed PSC is limited to 10 A, while for FOC and AISMPC, the saturation thresholds of the outer speed loop output are $\pm$10 A. The control parameters of the proposed PSC are listed in Table II. Note that the design of

TABLE I
SPMSM NOMINAL PARAMETERS

Parameter	Value
Nominal Stator Resistance R_s [Ohm]	0.95
Nominal Stator Inductance L_s [mH]	9.8
Nominal Rotor Flux Linkage ψ_f [Wb]	0.225
Rated Current I_n [A]	6.3
Rated Speed N_n [r/min]	3000
Rated Voltage V_n [V]	380
Motor Pole Pairs n_p [1]	3
Drive System Inertia J_m [Kgm^2]	7.78e-3

TABLE II
CONTROL PARAMETERS USED IN THE PROPOSED PSC

Parameter	k_{id}	k_ω	k_u	η_m	μ_ω^*	μ_d^*	ε
Value	1	2.5e-3	2.5e-4	250	2000	5	0.05

TABLE III
CONTROL PARAMETERS USED IN AISMPC

Parameter	k_s	c_s	k_q	c_q	k_d	c_d
Value	80	0.1	50	0.2	50	0.2

the integral coefficients is relatively easy, we can first choose a relatively small μ_d^* and design μ_ω^*, subsequently, where $\mu_\omega^* = (3p^2\psi_f(2+\eta_m T_s)/4J)\mu_d^*$. For AISMPC, the control parameters are listed in Table III. In the proposed PSC and AISMPC, a Kalman filter is used to estimate the load torque. For detailed information of the Kalman filter, the reader is referred to [29].

A. Verification of the Effectiveness of the Algebraically Designed Weighting Factors

Before we compare the performance of the proposed PSC with FOC and AISMPC, we have to know whether the algebraically designed weighting factors are effective. Following questions should be answered.

1) Do the calculated weighting factors contribute to satisfactory performance compared to weighting factors with values that differ from the proposed ones?
2) Is the proposed PSC sensitive to parameter mismatches? Specifically, are accurate parameters mandatory when calculating the weighting factors?

1) Advantage of the Algebraically Designed Weighting Factors Over Conventional the Trial-and-Error Tuning Procedure: To answer the first question, we need to compare the performance of PSC with different values in weighting factors and see whether (17) provides satisfactory (nearly optimal) performance. Fig. 4 illustrates the performance of PSC with different values in k_ω, where k_ω^* is the algebraically calculated weighting factor ($k_\omega^* = 2.5e\text{-}3$). Note that the machine parameters used to calculate k_ω^* are obtained from experimental tests and k_{id} is kept to 1. The reference speed is 1500 r/min and the load torque is 7.1 Nm.

As can be seen in Fig. 4, the system is unstable with $k_\omega = 0.2k_\omega^*$, where the ripples in i_q are extremely large. The performance improves as k_ω increases from $0.2k_\omega^*$ to $0.8k_\omega^*$. However, the increase of k_ω from k_ω^* to $2k_\omega^*$ results in larger i_d ripple. The performance of PSC with different weighting factor values is summarized in Table IV. It can be concluded

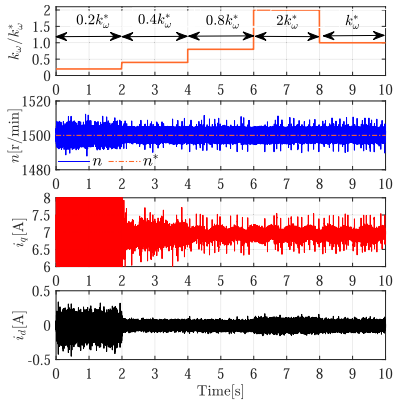

Fig. 4. Control performance of PSC with different values in weighting factor k_ω, from up to down are: ratio between the actual weighting factor k_ω and the proposed k_ω^*, motor speed, q-axis current, and d-axis current, respectively.

TABLE IV
PERFORMANCE OF PSC WITH DIFFERENT WEIGHTING FACTOR VALUES

Performance	$0.2k_\omega^*$	$0.4k_\omega^*$	$0.8k_\omega^*$	$2k_\omega^*$	k_ω^* (Prop.)
Speed ripples [r/min]	24.4	19.8	20.5	21.3	20.8
Ripples on i_q [A]	8.58	1.73	1.21	1.19	1.20
Ripples on i_d [A]	0.76	0.22	0.25	0.31	0.27

that the algebraically designed k_ω^* provides satisfactory (nearly optimal) performance compared to k_ω with different values, which is exactly the desired result in the trial-and-error tuning procedure. However, tremendous tuning effort is required in the trial-and-error method to obtain such satisfactory control performance.

2) Sensitivity of the Proposed PSC to Parameter Mismatches With Algebraically Designed Weighting Factors: To answer the second question, we need to change the inertia $\hat{J}_m$ and rotor flux $\hat{\psi}_f$ used in the prediction model as well as in the calculation of k_ω^*. If the performance of the proposed PSC varies within a small range, then the sensitivity to parameter mismatches is low. Fig. 5 shows the current total harmonic distortion (THD) and ripples in i_q and i_d with a set of different values in $\hat{J}_m$ and $\hat{\psi}_f$. The inertia $\hat{J}_m$ varies from J_m to $5J_m$, while the rotor flux $\hat{\psi}_f$ increases from ψ_f to $2\psi_f$. The rotor speed is 2400 r/min and the load torque is 7.1 Nm. As can be seen in the figure, the performance of the proposed PSC remains relatively similar with different parameter values. Thus, we conclude that the calculated weighting factors are feasible even in case of some parameter mismatches.

Remark 4: The variation of control performance under parameter mismatches is a common phenomenon in MPC, including PSC. Parameter mismatches could lead to the change of the control system feedback gain compared to the nominal case, which is reflected in the change of current THD and current ripples.

B. Comparison of Dynamic Performances

1) Acceleration Performances: Fig. 6 presents the acceleration performances of the proposed PSC, FOC, as well as AISMPC from standstill to 2400 r/min, where the load machine

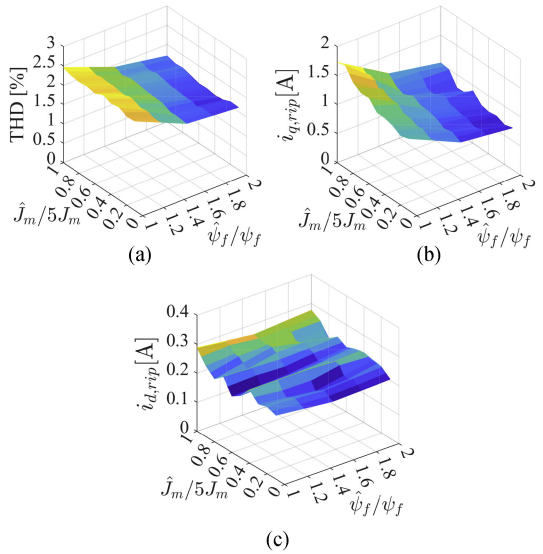

Fig. 5. Sensitivity of the proposed PSC to parameter mismatches with algebraically designed weighting factors (Speed: 2400 r/min, Load torque: 7.1 Nm). (a) Current THD. (b) Ripple in i_q. (c) Ripple in i_d.

TABLE V
ACCELERATION PERFORMANCES OF THE PROPOSED PSC, FOC, AND AISMPC

	Proposed PSC	FOC	AISMPC
Speed settling time [s]	0.151	0.154	0.163
Speed overshoot [r/min]	0	16.1	0
SSE of speed [r/min]	0	0	0

is powered OFF. For the proposed PSC, the rotor accelerates to the reference speed rapidly without overshoots (settling time: 0.151 s). The current i_q remains at the current limit (10 A) during the acceleration and decreases drastically as the speed error becomes relatively small. For FOC, the acceleration takes a longer time (0.154 s) with a speed overshoot of 16.1 r/min. Note that larger speed overshoot is expected if the PI coefficients are not well tuned, which is undesirable. At the beginning of the acceleration, overshoot in i_q is also observed. As the system enters quasi steady-state, i_q decreases gradually and a relatively large disturbance in i_d is noticeable. For AISMPC, the actual speed approaches its reference without overshoot. The acceleration time (0.163 s) is the longest one, which coincides with the results in [25]. The q-axis current descends slowly at the final stage of the acceleration. The acceleration performances of the proposed PSC, FOC, and AISMPC are listed in Table V.

2) Load Torque Disturbance Rejection Performances at Low Speed Operation: Fig. 7 shows the dynamic performances of three control schemes (i.e., the proposed PSC, FOC, and AISMPC) at 300 r/min with reference load torque step change from 0 to 7.1 Nm. Note that there are overshoots in the actual load torque since PI controllers are tuned based on magnitude optimum method for the load motor. The proposed PSC has the best disturbance rejection performance, demonstrated by the smallest speed drop (34.5 r/min) and shortest settle time (0.073 s). The reason lies in the fact that the speed error derivative is controlled in e_ω. In contrast, FOC yields the slowest dynamic response and the speed deviates from its reference heavily as the load torque applied. AISMPC outperforms FOC, but it is still inferior to the proposed PSC in terms of speed drop and settling time. Dynamic performances of the three control schemes under load torque change at 300 r/min are summarized in Table VI.

TABLE VI
DYNAMIC PERFORMANCES OF THE PROPOSED PSC, FOC, AND AISMPC UNDER SUDDEN LOAD TORQUE CHANGE AT 300 R/MIN

	Proposed PSC	FOC	AISMPC
Speed settling time [s]	0.073	0.102	0.095
Speed drop [r/min]	34.5	49.9	45.8
SSE of speed [r/min]	0	0	0
Speed ripples [r/min]	19.2/14.5	21.6/16.4	18.6/14.7
Ripples on i_q [A]	0.93/0.96	0.80/0.92	0.74/0.72
Ripples on i_d [A]	0.14/0.18	0.08/0.09	0.31/0.49
SSE of i_d [A]	0	0	0

TABLE VII
DYNAMIC PERFORMANCES OF THE PROPOSED PSC, FOC, AND AISMPC UNDER SUDDEN LOAD TORQUE CHANGE AT 2400 R/MIN

	Proposed PSC	FOC	AISMPC
Speed settling time [s]	0.142	0.201	0.160
Speed drop [r/min]	33.9	53.5	46.8
SSE of speed [r/min]	0	0	0
Speed ripples [r/min]	20.7/12.7	22.1/15.2	18.9/21.1
Ripples on i_q [A]	1.23/0.68	0.67/0.60	1.06/1.09
Ripples on i_d [A]	0.16/0.19	0.29/0.31	0.18/0.32
SSE of i_d [A]	0	0	0

3) Load Torque Disturbance Rejection Performances at High-Speed Operation: The dynamic responses of the proposed PSC, FOC, and AISMPC to load torque disturbance at 2400 r/min are shown in Fig. 8. At time instant 0.65 s, the reference load torque jumps from 0 to 7.1 Nm. Reminded that there are overshoots in the actual load torque. The proposed PSC exhibits once again the best load torque disturbance rejection performance. The settling time with the proposed PSC is 0.142 s, while FOC yields the longest recovery time (0.201 s). The overshoots in i_q are larger at high-speed operations than that at low-speed operations, which is because the overshoots in the actual load torque are larger. Comparative dynamic performances of the three control schemes under sudden load change at 2400 r/min are listed in Table VII.

C. Comparison of Steady-State Performances

1) Steady-State Performances at Low-Speed Operation: In Fig. 9, the stator currents and the corresponding spectra of the three control schemes (i.e., the proposed PSC, FOC, and AISMPC) at 300 r/min are shown. The load torque is 7.1 Nm. As shown in the figure, the phase currents can be well controlled with all the three control schemes, where the phase current spectra contain low harmonic components. However, the current THD with the proposed PSC is higher than those with FOC and AISMPC. The reason is that the bandwidth of the proposed PSC is the highest, where the effect of measurement errors could be amplified.

2) Steady-State Performances at High-Speed Operation: Fig. 10 shows the steady-state performances of the proposed PSC, FOC, and AISMPC at 2700 r/min with a load torque of 7.1

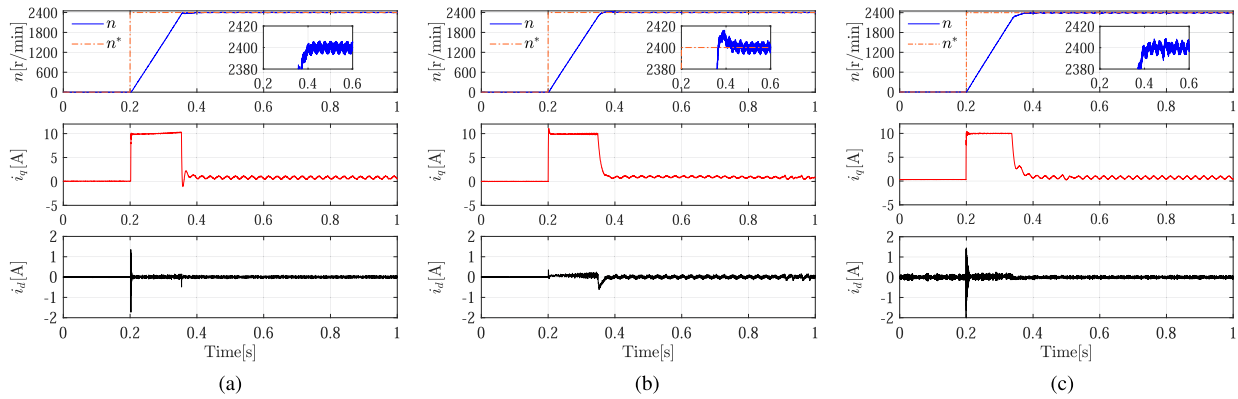

Fig. 6. Experimental results: Acceleration performances of the proposed PSC, FOC, and AISMPC, for each figure set, from up to down are: motor speed, q-axis current, and d-axis current, respectively. (a) Proposed PSC. (b) FOC. (c) AISMPC.

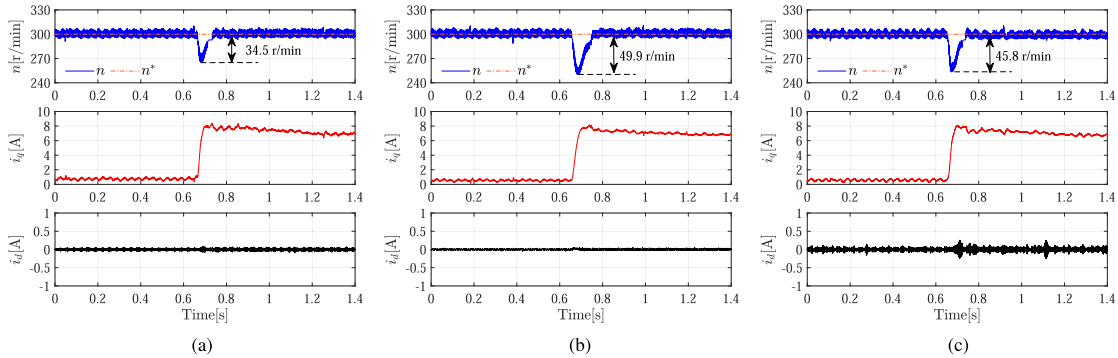

Fig. 7. Experimental results: Dynamic responses of the proposed PSC, FOC, and AISMPC under sudden load torque change at low speed operation, for each figure set, from up to down are: motor speed, q-axis current, and d-axis current, respectively. (a) Proposed PSC. (b) FOC. (c) AISMPC.

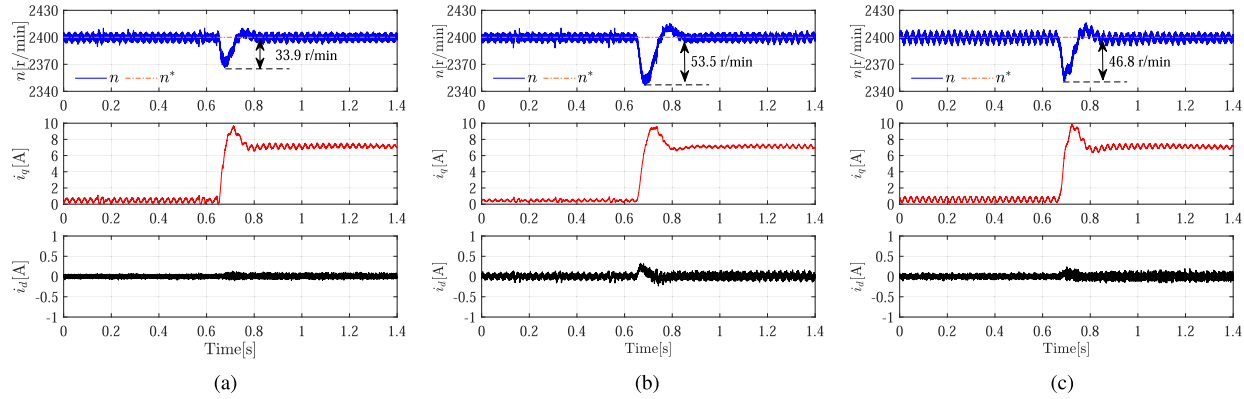

Fig. 8. Experimental results: Dynamic responses of the proposed PSC, FOC, and AISMPC under sudden load torque change at high-speed operation, for each figure set, from up to down are: motor speed, q-axis current, and d-axis current, respectively. (a) Proposed PSC. (b) FOC. (c) AISMPC.

Nm. Compared to Fig. 9, all of the current THD become higher for the three control schemes, where harmonics are clearly seen in the phase spectra. The proposed PSC yields the lowest current THD, thanks to its high feedback gain. FOC performs poorly because the high-frequency components cannot be well controlled by its low bandwidth PI controllers. The current THD of the proposed PSC, FOC, and AISMPC at 300 and 2700 r/min are listed in Table VIII.

D. Robustness of the Proposed PSC Against Parameter Mismatches

1) Robustness of the Proposed PSC Against Rotor Flux Linkage Mismatches: The performances of the proposed PSC and AISMPC under rotor flux linkage mismatches are shown in Fig. 11. The reference speed is 2400 r/min and the load torque is 7.1 Nm. Prior to the time instant 2 s, the rotor flux linkage used

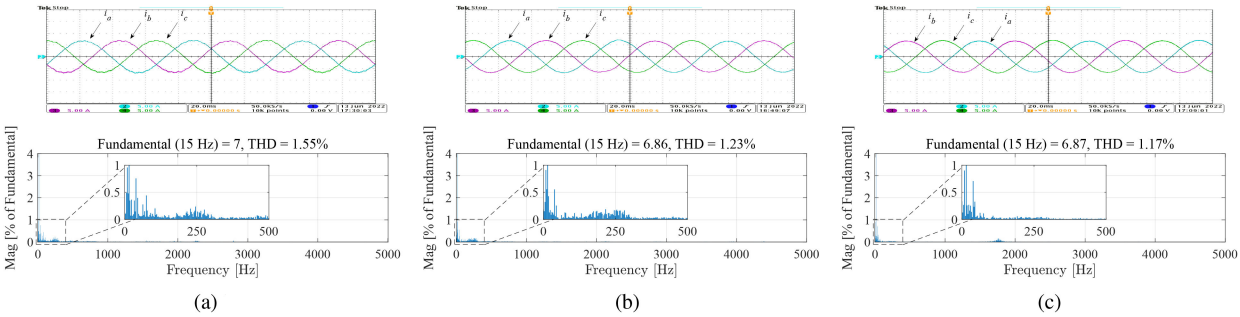

Fig. 9. Experimental results: Steady-state performances of the proposed PSC, FOC, and AISMPC at low-speed operation, for each figure set, from up to down are: phase currents and current spectrum, respectively. (a) Proposed PSC. (b) FOC. (c) AISMPC.

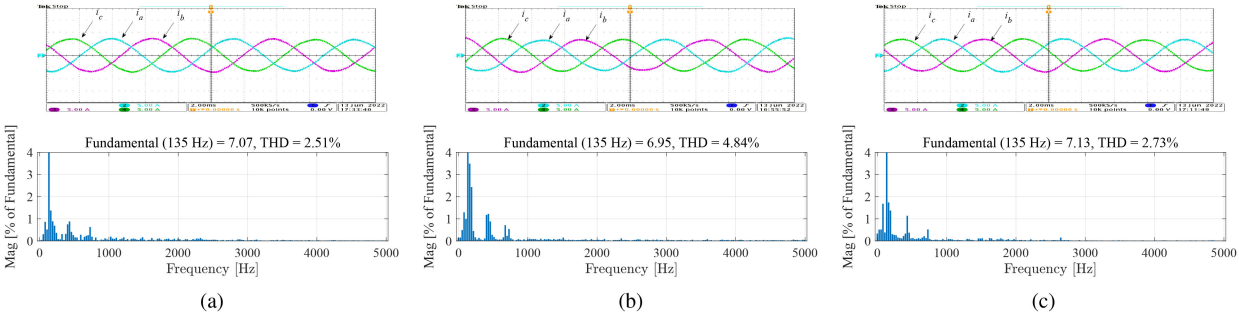

Fig. 10. Experimental results: Steady-state performances of the proposed PSC, FOC, and AISMPC at high-speed operation, for each figure set, from up to down are: phase currents and current spectrum, respectively. (a) Proposed PSC. (b) FOC. (c) AISMPC.

TABLE VIII
CURRENT THD OF THE PROPOSED PSC, FOC, AND AISMPC (LOAD TORQUE: 7.1 NM)

Speed [r/min]	Proposed PSC	FOC	AISMPC
300	1.55%	1.23%	1.17%
2700	2.51%	4.84%	2.73%

in the model is accurate (i.e., $\hat{\psi}_f = \psi_f$). From time instant 2–7 s, $\hat{\psi}_f$ changes stepwise from $0.5\psi_f$ to $2\psi_f$. After time instant 7 s, $\hat{\psi}_f$ stays at $2\psi_f$.

For the proposed PSC, the speed remains almost undisturbed, where only some spikes are seen at each switch point. On the contrary, obvious speed tracking error is obtained for AISMPC as $\hat{\psi}_f$ jumps. Moreover, long recovery time is required to eliminate the speed tracking errors. The speed errors are in the opposite variation direction of $\hat{\psi}_f$, which means the system is facing uncertainties. The system may become unstable at higher speed under heavier load. For high-speed operations, the accuracy of the $\hat{\psi}_f$ has great impact on the prediction accuracy. The back-EMF and the electromagnetic torque could be predicted with extremely large errors, which in turn affects the control action and the stability of the system. Fortunately, such inaccurate predictions can be compensated with the proposed PSC.

2) Robustness of the Proposed PSC Against Drive System Inertia Mismatches: In Fig. 12, the robustness of the proposed PSC against mismatches in J_m in both the prediction model and the Kalman filter is shown. The reference speed is 300 r/min and a sudden load from 0 to 7.1 Nm is applied at 0.3 s. As can be seen from the figure, the dynamic response is heavily related to $\hat{J}_m$. With $\hat{J}_m = 2J_m$, the speed drop is much larger than that with $\hat{J}_m = 0.5J_m$, which can be explained by the variation of the Kalman filter feedback gain caused by $\hat{J}_m$. Nonetheless, the reference speed can be well tracked at a steady state.

V. INFLUENCE OF THE INTEGRAL ACTIONS ON THE SYSTEM DYNAMIC PERFORMANCE

Until now, it is still unclear how the integral actions affect the dynamic performance of the proposed PSC. Specifically, we want to know whether the speed dynamic performance is affected by the integral term $S_\omega(k)$.

In this section, the influences of $S_\omega(k)$ on the acceleration performance and load torque disturbance rejection performance are investigated. The integral coefficient μ_ω^* is set to 0 and 2000, respectively. For $\mu_\omega^* = 0$, no integral action in e_ω is incorporated; For $\mu_\omega^* = 2000$, the past tracking errors of e_ω are incorporated as integral term.

The influence of $S_\omega(k)$ on the acceleration performance of the proposed PSC is shown in Fig. 13. Prior to the time instant 0.2 s, the motor is at standstill. At the instant 0.2 s, the reference speed jumps from 0 to 2400 r/min. As can be seen in the figure, the proposed PSC exhibits almost the same acceleration transients with different μ_ω^*, since the integral action is only activated

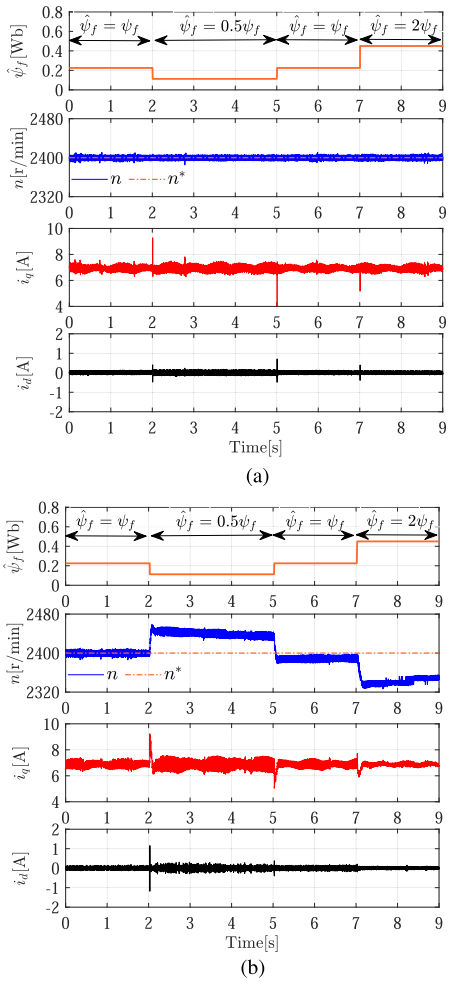

Fig. 11. Experimental results: Robustness of the proposed PSC and AISMPC against rotor flux linkage mismatches, for each figure-set, from up to down are: value of the rotor flux linkage used in the prediction model, motor speed, q-axis current, and d-axis current, respectively. (a) Proposed PSC. (b) AISMPC.

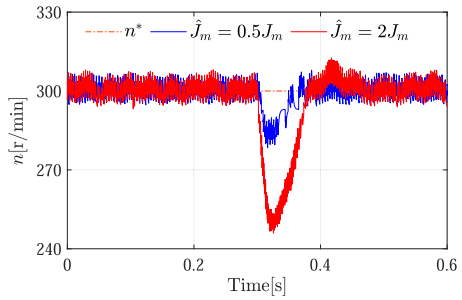

Fig. 12. Experimental results: Robustness of the proposed PSC against drive system inertia mismatches.

within a small range of the speed error ($\varepsilon = 0.05$). Strictly speaking, slightly faster transient performance is obtained with $\mu_\omega^* = 2000$. The reason is that as long as the integral action is activated, more control actions are required to reduce the speed error.

Fig. 14 shows the effect of $S_\omega(k)$ against sudden load torque change. The speed reference is 2400 r/min. At the time instant

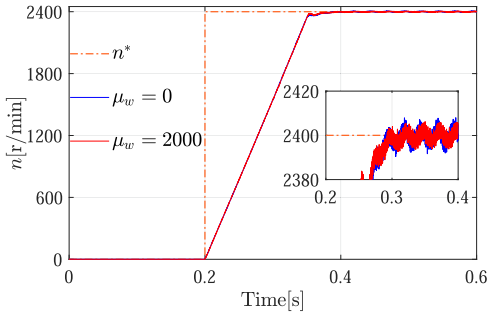

Fig. 13. Experimental results: Influence of the integral action on the acceleration performance.

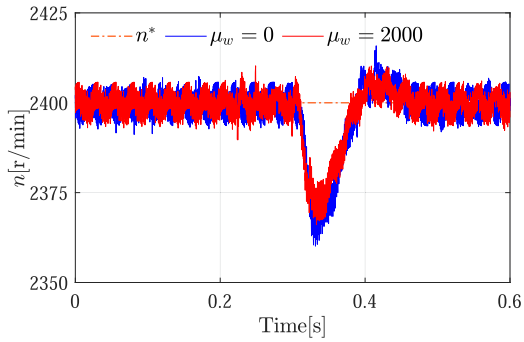

Fig. 14. Experimental results: Influence of integral action on load torque disturbance rejection performance.

TABLE IX
INFLUENCE OF INTEGRAL ACTION ON LOAD TORQUE DISTURBANCE REJECTION PERFORMANCE

	Speed settling time [s]	Speed drop [r/min]
$\mu_\omega^* = 2000$	0.142	33.9
$\mu_\omega^* = 0$	0.183	39.9

0.3 s, a load torque reference command from 0 to 7.1 Nm is given. It is obvious that $\mu_\omega^* = 2000$ yields better disturbance rejection performance. That is, the integral action contributes to less speed drop and shorter recovery time, which is summarized in Table IX.

VI. CONCLUSION

In this article, a PSC strategy has been proposed, where the weighting factors are designed algebraically and the steady-state errors are eliminated. The weighting factor for the d-axis current tracking error is simply set to 1, while the weighting factor for the equivalent speed tracking error is calculated based on the motor parameters. To eliminate the steady-state errors caused by model uncertainties and parameter mismatches, integral terms are incorporated into the cost function without incurring speed overshoots. Experimental results have validated the performance of the proposed PSC. Compared to FOC and AISMPC, the proposed PSC achieves better dynamic performance (e.g., shorter settling time), particularly during acceleration and load disturbance occurrence. Not to mention FOC yields undesirable speed overshoots. Meanwhile, the steady-state performance could also

benefit from the high feedback gain of the proposed PSC. At very high speed, the proposed PSC yields the lowest current THD among the three control schemes.

APPENDIX

This section proves that SSEs can be eliminated with the proposed PSC, even in the presence of model uncertainties.

The proof is straightforward. Based on the ideal reduced-order SPMSM model, the unconstrained reference voltage is calculated. This reference voltage is then substituted into the reduced-order model considering model uncertainties. In this way, the closed-loop transfer function under model uncertainties can be obtained. The steady-state gains are calculated subsequently to determine whether the SSEs can be eliminated.

A. Discrete Reduced-Order SPMSM Model

The discrete reduced-order SPMSM model can be described as [30]

$$\boldsymbol{x}(k+2)=\boldsymbol{x}(k+1)+\boldsymbol{H}\boldsymbol{U}_{dq}(k+1)+\boldsymbol{G}(k+1) \tag{29}$$

where

$$\boldsymbol{x}(k+1)=\begin{bmatrix} e_\omega(k+1) \\ i_d(k+1)\end{bmatrix}, \boldsymbol{U}_{dq}(k+1)=\begin{bmatrix} u_q(k+1) \\ u_d(k+1)\end{bmatrix}$$

$$\boldsymbol{H}=\begin{bmatrix} -\frac{3p^2\psi_f T_s}{2L_s J} & 0 \\ 0 & \frac{T_s}{L_s}\end{bmatrix}, \boldsymbol{G}(k+1)=\begin{bmatrix} g_\omega(k+1)T_s \\ g_d(k+1)T_s\end{bmatrix}$$

$$\begin{aligned} g_w(k+1)=\frac{3n_p^2\psi_f}{2J_m}\Bigg(&\left(\frac{R_s}{L_s}-\eta_m\right)i_q(k+1) \\ &+w_e(k+1)\left(i_d(k+1)+\frac{\psi_f}{L_s}\right)\Bigg) \\ &+\frac{\eta_m n_p}{J_m}T_L(k+1), \end{aligned}$$

$$g_d(k+1)=w_e(k+1)i_q(k+1)-\frac{R_s}{L_s}i_d(k+1).$$

B. Proof of SSEs Elimination With the Proposed PSC

The proposed PSC can be treated as a linear controller as long as the constraints are inactive. To ensure the constraints are not triggered, we have the following assumptions.

1) The relative speed error $|(\omega_e^*-\omega_e)/\omega_e^*|$ is within the specified range ε, where ε is small.
2) The dc-link voltage is sufficiently large so that the voltage constraints are not active.
3) The load torque does not result in overcurrents, i.e., the currents are within their constraints.

Under these assumptions, the reference voltage vector can be calculated analytically.

Based on the reduced-order SPMSM model (29), the cost function (19) can also be expressed as

$$\begin{aligned} J=&\Delta\boldsymbol{U}_{dq}^T(k+1)(\hat{\boldsymbol{H}}^T\hat{\boldsymbol{W}}\hat{\boldsymbol{H}}+k_u\boldsymbol{I}_2)\Delta\boldsymbol{U}_{dq}(k+1) \\ &-2\Delta\boldsymbol{U}_{dq}^T(k+1)\hat{\boldsymbol{H}}^T\hat{\boldsymbol{W}}\boldsymbol{\Gamma}(k+1) \\ &+\boldsymbol{\Gamma}(k+1)^T\hat{\boldsymbol{W}}\boldsymbol{\Gamma}(k+1) \end{aligned} \tag{30}$$

where $\hat{\boldsymbol{H}}$ and $\hat{\boldsymbol{W}}$ are the estimated matrices of $\boldsymbol{H}$ and $\boldsymbol{W}$, respectively. $\hat{\boldsymbol{H}}$ and $\hat{\boldsymbol{W}}$ are calculated with the motor nominal parameters, $\boldsymbol{I}_2$ is unit diagonal matrix. $\boldsymbol{\Gamma}(k+1)$ is defined as

$$\begin{aligned} \boldsymbol{\Gamma}(k+1)=&\boldsymbol{x}^*(k+2)+\boldsymbol{S}_{d\omega}(k)-\boldsymbol{x}(k+1) \\ &-\boldsymbol{G}(k+1)-\boldsymbol{H}\boldsymbol{U}_{dq}(k). \end{aligned}$$

where

$$\boldsymbol{S}_{d\omega}(k)=\begin{bmatrix} S_\omega(k) & S_d(k)\end{bmatrix}^T.$$

Since $\hat{\boldsymbol{H}}^T\hat{\boldsymbol{W}}\hat{\boldsymbol{H}}+k_u\boldsymbol{I}_2$ is positive definite, J can be minimized if the derivative of J with respect to $\Delta\boldsymbol{U}_{dq}$ is zero

$$\begin{aligned} \frac{\partial J}{\partial\Delta\boldsymbol{U}_{dq}}=&2(\hat{\boldsymbol{H}}^T\hat{\boldsymbol{W}}\hat{\boldsymbol{H}}+k_u\boldsymbol{I}_2)\Delta\boldsymbol{U}_{qd}(k+1) \\ &-2\hat{\boldsymbol{H}}^T\hat{\boldsymbol{W}}\boldsymbol{\Gamma}(k+1)=0. \end{aligned} \tag{31}$$

By solving (31), the unconstrained optimum incremental voltage is obtained

$$\Delta\boldsymbol{U}_{dq,\text{unc}}(k+1)=(\hat{\boldsymbol{H}}^T\hat{\boldsymbol{W}}\hat{\boldsymbol{H}}+k_u\boldsymbol{I}_2)^{-1}\hat{\boldsymbol{H}}^T\hat{\boldsymbol{W}}\boldsymbol{\Gamma}(k+1). \tag{32}$$

After substituting (32) into (29), $\boldsymbol{x}(k+2)$ follows as

$$\begin{aligned} \boldsymbol{x}(k+2)=&(\boldsymbol{I}_2-\boldsymbol{\xi}\boldsymbol{I}_2)(\boldsymbol{x}(k+1)+\boldsymbol{G}(k+1)+\boldsymbol{H}\boldsymbol{U}_{dq}(k)) \\ &+\boldsymbol{\xi}\boldsymbol{I}_2(\boldsymbol{x}^*(k+2)+\boldsymbol{S}_{d\omega}(k)) \end{aligned} \tag{33}$$

where $\boldsymbol{\xi}$ represents the model uncertainties

$$\boldsymbol{\xi}=\boldsymbol{H}(\hat{\boldsymbol{H}}^T\hat{\boldsymbol{W}}\hat{\boldsymbol{H}}+k_u\boldsymbol{I}_2)^{-1}\hat{\boldsymbol{H}}^T\hat{\boldsymbol{W}}=\begin{bmatrix} \xi_\omega & 0 \\ 0 & \xi_d\end{bmatrix}.$$

Neglect the term $(\boldsymbol{I}_2-\boldsymbol{\xi}\boldsymbol{I}_2)(\boldsymbol{G}(k+1)+\boldsymbol{H}\boldsymbol{U}_{dq}(k))$ and apply z-transformation to (33), we have

$$\begin{aligned} \begin{bmatrix} z^2E_\omega(z) \\ z^2I_d(z)\end{bmatrix}=&\begin{bmatrix} z(1-\xi_\omega)E_\omega(z) \\ z(1-\xi_d)I_d(z)\end{bmatrix} \\ &+\begin{bmatrix} \xi_\omega(z^2E_\omega^*(z)+\frac{\mu_\omega T_s z}{z-1}(E_\omega^*(z)-E_\omega(z))) \\ \xi_d(z^2I_d^*(z)+\frac{\mu_\omega T_s z}{z-1}(I_d^*(z)-I_d(z)))\end{bmatrix}. \end{aligned} \tag{34}$$

Based on (34), the closed-loop transfer function can be interpreted as

$$\begin{bmatrix} \frac{E_\omega(z)}{E_\omega^*(z)} \\ \frac{I_d(z)}{I_d^*(z)}\end{bmatrix}=\begin{bmatrix} \frac{\xi_\omega(z^2-z+\mu_\omega T_s)}{z^2+(\xi_\omega-2)z+(1-\xi_\omega+\xi_\omega\mu_\omega T_s)} \\ \frac{\xi_d(z^2-z+\mu_d T_s)}{z^2+(\xi_d-2)z+(1-\xi_d+\xi_d\mu_d T_s)}\end{bmatrix}. \tag{35}$$

The steady-state gain of the proposed PSC can be obtained by setting $z=1$ in (35)

$$\begin{bmatrix} \frac{E_\omega(1)}{E_\omega^*(1)} \\ \frac{I_d(1)}{I_d^*(1)}\end{bmatrix}=\begin{bmatrix} 1 \\ 1\end{bmatrix}. \tag{36}$$

As can be seen from (36), SSEs can be eliminated with the proposed PSC even in case of model uncertainties.

REFERENCES

[1] J. Rodriguez et al., "State of the art of finite control set model predictive control in power electronics," *IEEE Trans. Ind. Inform.*, vol. 9, no. 2, pp. 1003–1016, May 2013.

[2] S. Vazquez, J. Rodriguez, M. Rivera, L. G. Franquelo, and M. Norambuena, "Model predictive control for power converters and drives: Advances and trends," *IEEE Trans. Ind. Electron.*, vol. 64, no. 2, pp. 935–947, Feb. 2017.

[3] C. S. Lim, E. Levi, M. Jones, N. A. Rahim, and W. P. Hew, "FCS-MPC-based current control of a five-phase induction motor and its comparison with PI-PWM control," *IEEE Trans. Ind. Electron.*, vol. 61, no. 1, pp. 149–163, Jan. 2014.

[4] J. A. Riveros, F. Barrero, E. Levi, M. J. Durán, S. Toral, and M. Jones, "Variable-speed five-phase induction motor drive based on predictive torque control," *IEEE Trans. Ind. Electron.*, vol. 60, no. 8, pp. 2957–2968, Aug. 2013.

[5] E. Fuentes, D. Kalise, J. Rodríguez, and R. M. Kennel, "Cascade-free predictive speed control for electrical drives," *IEEE Trans. Ind. Electron.*, vol. 61, no. 5, pp. 2176–2184, May 2014.

[6] J. Rodriguez, R. M. Kennel, J. R. Espinoza, M. Trincado, C. A. Silva, and C. A. Rojas, "High-performance control strategies for electrical drives: An experimental assessment," *IEEE Trans. Ind. Electron.*, vol. 59, no. 2, pp. 812–820, Feb. 2012.

[7] P. Cortes et al., "Guidelines for weighting factors design in model predictive control of power converters and drives," in *Proc. IEEE Int. Conf. Ind. Technol.*, 2009, pp. 1–7.

[8] S. A. Davari, D. A. Khaburi, and R. Kennel, "An improved FCS-MPC algorithm for an induction motor with an imposed optimized weighting factor," *IEEE Trans. Power Electron.*, vol. 27, no. 3, pp. 1540–1551, Mar. 2012.

[9] T. Geyer, "Algebraic tuning guidelines for model predictive torque and flux control," *IEEE Trans. Ind. Appl.*, vol. 54, no. 5, pp. 4464–4475, Sep./Oct. 2018.

[10] Y. Zhang, H. Yang, and B. Xia, "Model-predictive control of induction motor drives: Torque control versus flux control," *IEEE Trans. Ind. Appl.*, vol. 52, no. 5, pp. 4050–4060, Sep./Oct. 2016.

[11] M. Xiao, T. Shi, Y. Yan, W. Xu, and C. Xia, "Predictive torque control of permanent magnet synchronous motors using flux vector," *IEEE Trans. Ind. Appl.*, vol. 54, no. 5, pp. 4437–4446, Sept./Oct. 2018.

[12] C. A. Rojas, J. Rodriguez, F. Villarroel, J. R. Espinoza, C. A. Silva, and M. Trincado, "Predictive torque and flux control without weighting factors," *IEEE Trans. Ind. Electron.*, vol. 60, no. 2, pp. 681–690, Feb. 2013.

[13] M. Siami, H. K. Savadkoohi, A. Abbaszadeh, D. A. Khaburi, J. Rodriguez, and M. Rivera, "Predictive torque control of a permanent magnet synchronous motor fed by a matrix converter without weighting factor," in *Proc. 7th Power Electron. Drive Syst. Technol. Conf.*, 2016, pp. 614–619.

[14] M. Norambuena, J. Rodriguez, Z. Zhang, F. Wang, C. Garcia, and R. Kennel, "A very simple strategy for high-quality performance of AC machines using model predictive control," *IEEE Trans. Power Electron.*, vol. 34, no. 1, pp. 794–800, Jan. 2019.

[15] Y. Zhang, B. Zhang, H. Yang, M. Norambuena, and J. Rodriguez, "Generalized sequential model predictive control of IM drives with field-weakening ability," *IEEE Trans. Power Electron.*, vol. 34, no. 9, pp. 8944–8955, Sep. 2019.

[16] P. R. U. Guazzelli, W. C. de Andrade Pereira, C. M. R. de Oliveira, A. G. de Castro, and M. L. de Aguiar, "Weighting factors optimization of predictive torque control of induction motor by multiobjective genetic algorithm," *IEEE Trans. Power Electron.*, vol. 34, no. 7, pp. 6628–6638, Jul. 2019.

[17] M. Novak, H. Xie, T. Dragicevic, F. Wang, J. Rodriguez, and F. Blaabjerg, "Optimal cost function parameter design in predictive torque control (PTC) using artificial neural networks (ANN)," *IEEE Trans. Ind. Electron.*, vol. 68, no. 8, pp. 7309–7319, Aug. 2021.

[18] M. Preindl and S. Bolognani, "Model predictive direct speed control with finite control set of PMSM drive systems," *IEEE Trans. Power Electron.*, vol. 28, no. 2, pp. 1007–1015, Feb. 2013.

[19] E. J. Fuentes, C. Silva, D. E. Quevedo, and E. I. Silva, "Predictive speed control of a synchronous permanent magnet motor," in *Proc. IEEE Int. Conf. Ind. Technol.*, Feb. 2009, pp. 1–6.

[20] J. Rodríguez, M. A. Pérez, H. Young, and H. Abu-Rub, "Model predictive speed control of electrical machines," *Power Electronics for Renewable Energy Systems, Transportation and Industrial Applications.*Piscataway, NJ, USA: IEEE Press, 2014, pp. 608–629.

[21] P. Kakosimos and H. Abu-Rub, "Predictive speed control with short prediction horizon for permanent magnet synchronous motor drives," *IEEE Trans. Power Electron.*, vol. 33, no. 3, pp. 2740–2750, Mar. 2018.

[22] X. Zhang and Y. He, "Direct voltage-selection based model predictive direct speed control for PMSM drives without weighting factor," *IEEE Trans. Power Electron.*, vol. 34, no. 8, pp. 7838–7851, Aug. 2019.

[23] X. Zhang, Y. Cheng, Z. Zhao, and Y. He, "Robust model predictive direct speed control for SPMSM drives based on full parameter disturbances and load observer," *IEEE Trans. Power Electron.*, vol. 35, no. 8, pp. 8361–8373, Aug. 2020.

[24] H. T. Nguyen and J. Jung, "Finite control set model predictive control to guarantee stability and robustness for surface-mounted pm synchronous motors," *IEEE Trans. Ind. Electron.*, vol. 65, no. 11, pp. 8510–8519, Nov. 2018.

[25] Z. Li, F. Wang, D. Ke, J. Li, and W. Zhang, "Robust continuous model predictive speed and current control for PMSM with adaptive integral sliding-mode approach," *IEEE Trans. Power Electron.*, vol. 36, no. 12, pp. 14398–14408, Dec. 2021.

[26] L. Wang, S. Chai, D. Yoo, L. Gan, and K. Ng, "Discrete-time model predictive control (DMPC) of electrical drives and power converter," in *PID and Predictive Control of Electrical Drives and Power Converters using MATLAB / Simulink*. Piscataway, NJ, USA: IEEE Press, 2015, pp. 265–284.

[27] J. Jung, V. Q. Leu, T. D. Do, E. Kim, and H. H. Choi, "Adaptive PID speed control design for permanent magnet synchronous motor drives," *IEEE Trans. Power Electron.*, vol. 30, no. 2, pp. 900–908, Feb. 2015.

[28] X. Liu, L. Zhou, J. Wang, X. Gao, Z. Li, and Z. Zhang, "Robust predictive current control of permanent-magnet synchronous motors with newly designed cost function," *IEEE Trans. Power Electron.*, vol. 35, no. 10, pp. 10778–10788, Oct. 2020.

[29] X. Gao, M. Abdelrahem, C. M. Hackl, Z. Zhang, and R. Kennel, "Direct predictive speed control with a sliding manifold term for pmsm drives," *IEEE Trans. Emerg. Sel. Topics Power Electron.*, vol. 8, no. 2, pp. 1258–1267, Jun. 2020.

[30] X. Liu et al., "Continuous control set predictive speed control of spmsm drives with short prediction horizon," *IEEE Trans. Power Electron.*, vol. 37, no. 9, pp. 10166–10177, Sep. 2022.

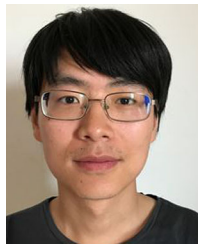

Xicai Liu (Member, IEEE) received the double M.S. degree in control engineering from Tongji University, Shanghai, China and Technische Universitaet Muenchen, Munich, Germany, in 2013, and the Ph.D. degree in electrical engineering from the Huazhong University of Science and Technology (HUST), Wuhan, China, in 2021.

Since 2014, he has been with the HUST. His main research interests include predictive control of electrical drives and power electronics.

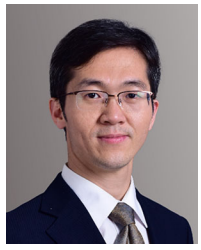

Jin Wang (Member, IEEE) received the B.S., M.S., and Ph.D. degrees in electrical engineering from the Huazhong University of Science and Technology, Wuhan, China, in 2002, 2005, and 2010, respectively.

From 2010 to 2013, he was a Postdoctoral Fellow with the Huazhong University of Science and Technology, where he is currently an Associate Professor. His research interests include design and control of permanent-magnet brushless machines.

Xiaonan Gao (Member, IEEE) was born in Liaoning, China, in 1990. He received the B.S. and M.S. degrees in electrical engineering from the Dalian University of Technology, Dalian, China, in 2013 and 2016, respectively. He is currently working toward the Ph.D. degree with the Institute for Electrical Drive Systems and Power Electronics, Technical University of Munich, Munich, Germany.

His research interests include power electronics and electrical drives, predictive control, and multilevel converters.

Wei Tian (Member, IEEE) was born in Taizhou, Jiangsu, China, in 1989. He received the B.Eng. degree in electrical engineering and automation from Central South University, Changsha, China, in 2012, and the M.Sc. degree in electrical power engineering from RWTH Aachen University, Aachen, Germany, in 2015. Since 2016, he has been working toward the Ph.D. degree with the Chair of Electrical Drive Systems and Power Electronics, Technical University of Munich, Munich, Germany.

His research interests include power electronics and electrical drives, model predictive control, and modular multilevel converter.

Libing Zhou (Member, IEEE) received the B.S., M.S., and Ph.D. degrees in electrical engineering from the Huazhong University of Science and Technology, Wuhan, China, in 1982, 1985, and 1993, respectively.

He is currently a Professor with the Huazhong University of Science and Technology, Wuhan. His research interests include electromagnetic design, operation analysis, and drives of ac machines.

Ralph Kennel (Senior Member, IEEE) was born in Kaiserslautern, Germany, in 1955. He received the Diploma and Dr. Ing. (Ph.D.) degrees in electrical engineering from the University of Kaiserslautern, Kaiserslautern, Germany, in 1979 and 1984, respectively.

From 1983 to 1999, he worked on several positions with Robert BOSCH GmbH, Germany. Until 1997, he was responsible for the development of servo drives. From 1994 to 1999, he was a Visiting Professor with the University of Newcastle-upon-Tyne, Newcastle-upon-Tyne, U.K. From 1999 to 2008, he was a Professor of electrical machines and drives with Wuppertal University, Wuppertal, Germany. Since 2008, he has been a Professor of electrical drive systems and power electronics with the Technical University of Munich, Munich, Germany. His current main research interests include renewable energy systems, sensorless control of ac drives, predictive control of power electronics, and hardware-in-the-loop systems.

Prof. Kennel is a Fellow of the IEE and a Chartered Engineer in the U.K. within IEEE. He is a Treasurer of the Germany Section as well as ECCE Global Partnership Chair of the Power Electronics society.